



CHORUS

This is the accepted manuscript made available via CHORUS. The article has been published as:

Hydration-dependent dynamics of deeply cooled water under strong confinement

C. E. Bertrand, K.-H. Liu, E. Mamontov, and S.-H. Chen

Phys. Rev. E **87**, 042312 — Published 26 April 2013

DOI: [10.1103/PhysRevE.87.042312](https://doi.org/10.1103/PhysRevE.87.042312)

Hydration dependent dynamics of deeply-cooled water under strong confinement

C. E. Bertrand,¹ K.-H. Liu,^{1,2} E. Mamontov,³ and S.-H. Chen^{1,*}

¹*Department of Nuclear Science & Engineering, Massachusetts Institute of Technology, Cambridge, MA 02139*

²*Institute of Atomic & Molecular Sciences, Academia Sinica, Taipei 10617, Taiwan*

³*Neutron Sciences Directorate, Oak Ridge National Laboratory, Oak Ridge, TN 37831*

(Dated: April 11, 2013)

We have measured the hydration-level dependence of the single particle dynamics of water confined in the ordered mesoporous silica MCM-41. The dynamic crossover observed at full hydration is absent at monolayer hydration. The monolayer dynamics are significantly slower than those of water in a fully hydrated pore at ambient temperatures. At low temperatures, the opposite is found to be true. These results underscore the importance of water's tetrahedral hydrogen-bond network in accounting for its low temperature dynamic properties.

PACS numbers: 61.05.fg, 61.20.Lc, 66.30.jj

I. INTRODUCTION

Dynamic and structural properties of deeply-cooled water under strong confinement have garnered significant attention in recent years [1–4]. *Strongly-confined* water does not crystallize at temperatures below the bulk homogeneous nucleation limit ($\simeq 235$ K at 1 atm): a region of the phase diagram we label *deeply-cooled* [5]. Hence, liquid state properties of strongly-confined water can be probed at state points that are not accessible to the bulk phase, albeit at the cost of introducing strong surface interactions and finite-size effects.

Previous quasielastic neutron scattering (QENS) measurements of the single-particle dynamics of water under strong confinement in the mesoporous silica material MCM-41 found a dynamic crossover at $T_x \simeq 225$ K [6]. The temperature dependence of the long-time relaxation was found to be super-Arrhenius above T_x , but Arrhenius below T_x . This phenomenon was originally identified as a *fragile-to-strong crossover*, however, because the semantics of this title raise some hackles [7–9], we will simply call it a *dynamic crossover*. Subsequent nuclear magnetic resonance (NMR) spectroscopy measurements have confirmed the dynamic crossover in MCM-41 confined water [10], but dielectric spectroscopy measurements do not find an abrupt change in the temperature dependence of the observed relaxation time [11].

The dynamic crossover has been interpreted in terms of a hypothetical liquid-liquid phase transition in bulk supercooled water [12]. However, the extent to which the properties of strongly-confined water can be viewed as an extrapolation of bulk properties remains a topic of debate [1, 13]. Understanding the effects of confinement is essential to establishing any connection between bulk and confined water.

In order to probe the role of surface interactions in strongly-confined water, several investigators have studied the hydration dependence of water dynamics in vari-

ous confining media such as clays [14–17] and oxides [18–21] via neutron scattering. At low hydration levels, a majority of water molecules are in close proximity to the surface of the confining substrate. Consequently, the dynamics at low hydration more strongly reflect the interaction between water and substrate. The recent findings of Mamontov *et al.* [21], who studied water confined in rutile (TiO_2) via QENS, are particularly relevant to the present work. At high hydration, these authors observed a dynamic crossover, like that found in fully hydrated MCM-41. However, at low hydration, the relaxation times are Arrhenius over the experimental temperature range. A similar distinction between confined water dynamics at high and low hydration was seen in Yoshida *et al.*'s [22, 23] neutron spin echo (NSE) spectroscopy studies of water confined in MCM-41. For full hydration, a dynamic crossover was seen, while Arrhenius behavior was found at low hydration.

In the case of rutile, the low hydration dynamics were found to be slower than the full hydration dynamics at high temperatures, but faster at low temperatures [21]. The relative slowness of the low hydration dynamics is indicative of strong interactions between water and rutile. Surprisingly, the low hydration water was generally found to relax more quickly at all temperatures in the NSE measurements of Yoshida *et al.* [23]. This is unexpected, since the interactions between the silica surface of MCM-41 and water are strongly hydrophilic.

Here we report measurements of the single-particle dynamics of water in MCM-41 for monolayer and fully hydrated states. Our study compliments previous neutron scattering measurements of hydration dependent dynamics in other confining substrates. It also allows us to address whether the low hydration dynamics are in fact “fast” in MCM-41. We have confirmed the absence of a dynamic crossover for monolayer hydration and have characterized the monolayer dynamics. Finally, we have found that monolayer water is in fact slower than full hydration water at high temperatures, but faster at low temperatures.

* Corresponding author: sowhsin@mit.edu

II. EXPERIMENT

Synthesis of MCM-41-S-15 was performed following a previously described protocol [24]. MCM-41-S-15 powder consists of micron-sized grains, each of which is formed from a hexagonal array of cylindrical silica pores. While the average pore length is comparable to the grain size, the average diameter of the pores, as determined by a Barrett-Joyner-Halenda (BJH) analysis [25], is 1.5 ± 0.2 nm. This value is useful for comparison with other BJH diameters, but may underestimate a more geometric definition of the pore diameter. Regardless, water confined in our sample does not exhibit the melting peak indicative of crystallization in differential scanning calorimetry measurements and is therefore strongly confined. Samples were hydrated by exposing dry MCM-41-S-15 powder to water vapor in a sealed container. Two hydration levels, as characterized by weight gain, were studied: monolayer hydration ($0.10 \text{ gH}_2\text{O/gMCM}$) and full hydration ($0.43 \text{ gH}_2\text{O/gMCM}$). The adsorption isotherm data presented in Fig. 1 justifies these designations. Due to the silica

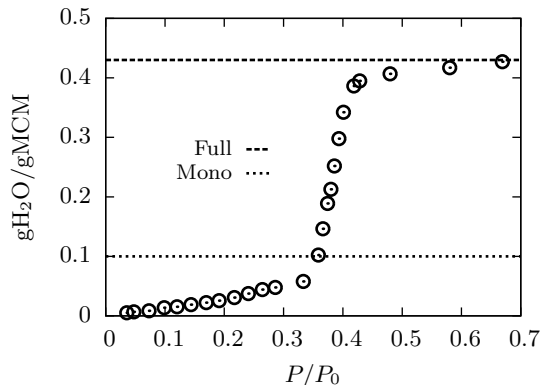


FIG. 1. Isothermal adsorption of water vapor onto MCM-41-S-15 at $T = 298$ K (adapted from [26]). The two plateaus seen at relative pressures of $P/P_0 \lesssim 0.35$ and $P/P_0 \gtrsim 0.45$ are characteristic of monolayer water adsorption and capillary condensation respectively. The horizontal lines mark the two hydration levels used in the experiment.

composition of MCM-41-S-15, the majority of water resides on the surface of the pores for monolayer hydration. This picture is supported by MD simulations [27]. At full hydration, the pores are filled, with negligible external water [28].

QENS is an ideal probe for investigating the single-particle dynamics of water confined in MCM-41. Due to the exceptionally large incoherent neutron scattering cross-section of hydrogen, QENS essentially probes the self-dynamic structure factor of the confined water's hydrogen atoms. QENS measurements were performed on the near-backscattering spectrometer BASIS [29] at the Spallation Neutron Source at Oak Ridge National Lab. BASIS has a Q -averaged energy resolution of $3.4 \mu\text{eV}$

(Full width at half max) and an effective dynamic range of $\pm 100 \mu\text{eV}$. QENS spectra were measured at Q values between $3 - 19 \text{ nm}^{-1}$, where Q is the magnitude of the wavevector transfer, and in the temperature range $T = 290 \text{ K} - 180 \text{ K}$. Examples of measured spectra are shown in Fig. 2.

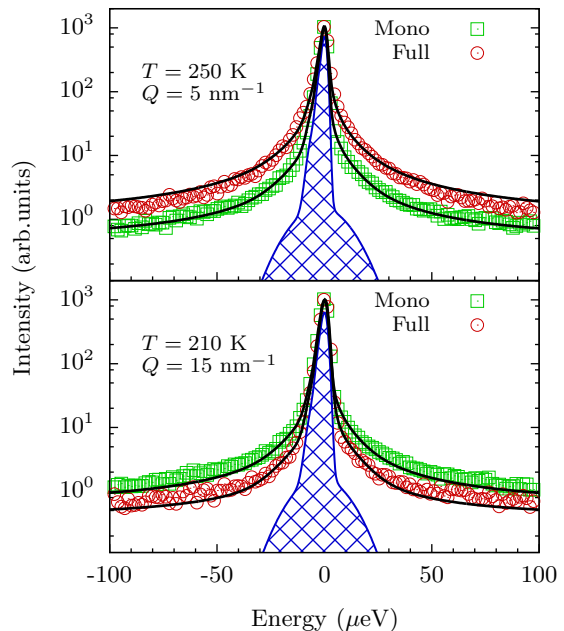


FIG. 2. (Color online) Normalized QENS spectra at two temperatures. The width of each spectrum is roughly proportional to the decay rate of the system. Monolayer water is seen to relax more slowly than full hydration water at 250 K , whereas this ordering is reversed at 210 K . Solid curves are fits with Eqs. (1) and (3). The filled solid curve is the elastic contribution to the monolayer scattering.

III. RESULTS

Measured scattering intensities, at energy transfer E , were fit with the following model

$$I(E) = \{p\delta(E) + (1-p)\mathcal{F}[F_s(t)]\} \otimes R(E) + B, \quad (1)$$

where \mathcal{F} denotes a time Fourier transform, \otimes is the convolution operator, $R(E)$ is the instrumental resolution function, and B is a background constant. The elastic fraction p , which is not present in bulk water, can be partially attributed to immobile hydrogens in surface silanol groups. The self-intermediate scattering function (SISF) $F_s(t)$ is related to the position $\mathbf{r}_j(t)$ of the j -th hydrogen atom at time t by

$$F_s(Q, t) = \left\langle \sum_j \exp(i\mathbf{Q} \cdot [\mathbf{r}_j(t) - \mathbf{r}_j(0)]) \right\rangle, \quad (2)$$

where the brackets denote an ensemble average and \mathbf{Q} is the wavevector transfer.

Spectra collected at 10 K were used for the instrumental resolution function. A combination of four Gaussians and a constant background provide an adequate description of $R(E)$, except at $Q = 19 \text{ nm}^{-1}$, which was omitted from the analysis. The constant B was approximated by the Q -averaged background from these fits, with $B_{\text{mono}} = 1.6 \pm 0.3$ and $B_{\text{full}} = 0.69 \pm 0.07$, where the units match those of Fig. 2.

The decay of $F_s(t)$ is believed to occur in two steps [27]. An illustrative SISF from a previous molecular dynamics simulation of water confined in MCM-41 is shown in Fig. 3. The first step corresponds to localized ‘‘cage-rattling’’

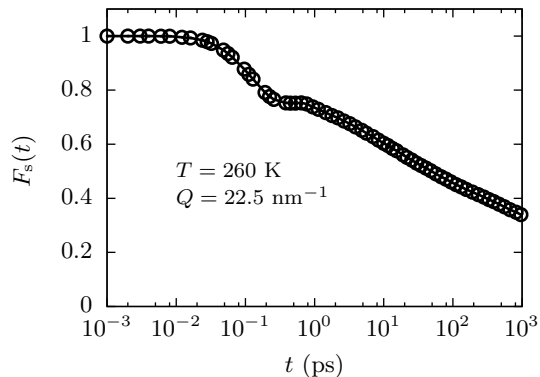


FIG. 3. Self intermediate scattering function of SPC/E water confined in a silica pore of diameter 1.5 nm (adapted from [30]). The long time relaxation is highly non-exponential. $F_s(t)$ was calculated using only the water oxygen atoms. This eliminates contributions from short-time molecular rotations.

and occurs on sub-picosecond time scales. These motions are generally beyond the dynamic range of the spectrometer and include ballistic and rotational processes. The second (long-time) step is highly non-exponential with a strongly temperature dependent relaxation time. To account for these physical considerations, the experimental SISF is taken to be of the form

$$F_s(t) \simeq A(Q) \exp[-(\Gamma t)^\beta], \quad (3)$$

where $A(Q)$ is the amplitude after the initial step, Γ is the decay rate and β is a stretching exponent. Single-particle motion in confinement also results in a Q -dependent elastic component in $F_s(t)$ [31]. Such a contribution can be absorbed into p .

If left free, the fitting parameters in Eqs. (1) and (3), namely, p , A , Γ , and β , are strongly correlated. We have constrained two of these parameters to regularize the fit. First, the stretching exponent has been fixed at $\beta = 0.5$. This is the same value adopted by Yoshida *et al.* [23] and it is consistent with previous work on fully hydrated pores [6]. We have taken the elastic fraction to be of the

form $p(Q) = p_0 A(Q)$, with p_0 constant. This approximation accounts for the fact that both $p(Q)$ and $A(Q)$ are expected to have the form of a Debye-Waller factor. The spectra at 290K, where the elastic fraction p is most easily distinguished, were fit first. Values of p_0 obtained from these fits were Q -averaged and fixed at $p_{0,\text{mono}} = 0.59$ and $p_{0,\text{full}} = 0.23$. Not surprisingly, the elastic fraction is greater in the monolayer case, where bound silanol hydrogens make up a greater fraction of the total number of incoherent scatters. At each Q and T the spectra were fit with this constrained model. With only two free parameters (A and Γ) the optimization problem is well-conditioned and yields results that are insensitive to the choice of initial parameters. The decay rates extracted from these fits are presented in Fig. 4.

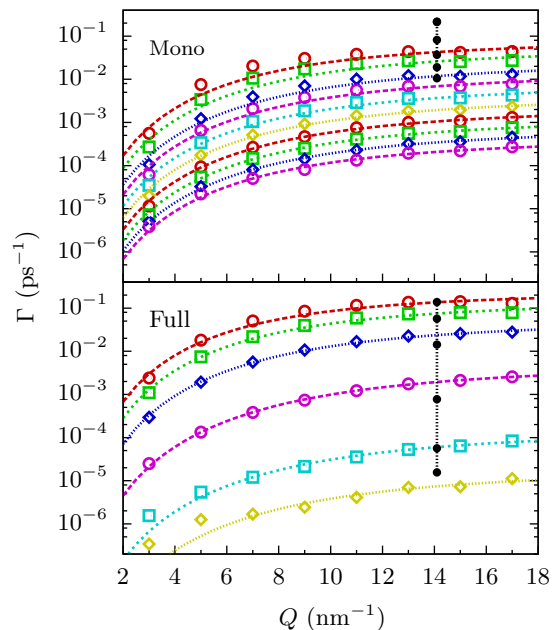


FIG. 4. (Color online) Decay rates extracted from fits of the QENS spectra with Eqs. (1) and (3). The points correspond to the following temperatures. Monolayer: (from top to bottom) 290, 270, 250, 240, 230, 220, 210, 200, 190, and 180 K. Full hydration: (from top to bottom) 290, 270, 250, 230, 210, and 190 K. The curves are fits with Eq. (4). The filled points connected by a vertical line at $Q = 14.1 \text{ nm}^{-1}$ are taken from the work of Yoshida *et al.* [23] and correspond to the same temperatures as our full hydration case. For monolayer hydration, the filled points at 290 K and 270 K completely overlap.

Both the monolayer and full hydration decay rates increase monotonically with Q and T . Notably, Γ appears to saturate at high values of Q . This behavior is similar to that observed in bulk supercooled water, where the long time decay is well described by a jump diffusion model [32]. Hence, we have fit the decay rates with the

function

$$\Gamma(Q) = \frac{1}{\tau} \left[\frac{(\ell Q)^2}{1 + (\ell Q)^2} \right]^{1/\beta}. \quad (4)$$

In the limit $\beta \rightarrow 1$, this equation corresponds to a simple jump diffusion model with residence time τ and an exponential distribution of jump lengths, where the average jump length is ℓ . We have raised the term in square brackets to the power $1/\beta$ so that the SISF remains Gaussian in Q as $Q \rightarrow 0$. The resulting fit curves are plotted in Fig. 4. Previous studies of water in Na-vermiculite clay [14] and in ZrO_2 [20] have successfully fit the measured decay rates with a jump diffusion model based on a gaussian distribution of jump lengths.

The temperature dependence of the Q -independent relaxation times τ is shown in Fig. 5. The monolayer re-

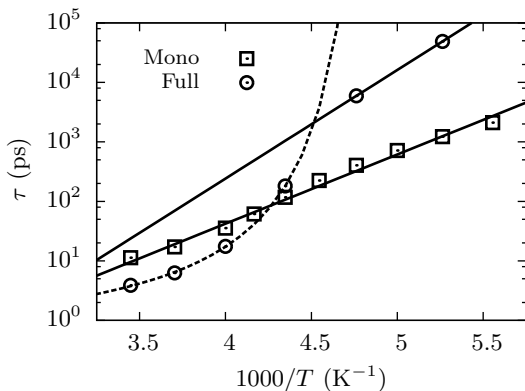


FIG. 5. Relaxation times extracted from fits of the Q -dependent decay rates with Eq. (4). Straight lines are fits to Eq. (5). The dashed curve is a fit to Eq. (6). The relaxation time of the monolayer water is well described by the Arrhenius law at all temperatures, whereas the full hydration water exhibits a dynamic crossover at $T_x \simeq 220$ K. At temperatures above ~ 230 K, the monolayer water relaxes more slowly than the full hydration case. Below this temperature, the opposite is true.

laxation times are well described by an Arrhenius law

$$\tau = \tau_0 \exp\left(\frac{E_a}{k_B T}\right), \quad (5)$$

where τ_0 is the relaxation time at $T \rightarrow \infty$, E_a is the activation energy for the relaxation process, and k_B is Boltzmann's constant. In this case, the extracted activation energy is $E_a = 22$ kJ/mol. The full hydration relaxation times have been fit in the typical manner [6]. For temperatures below 225 K, the relaxation times were fit with the Arrhenius law, whereas the super-Arrhenius behavior observed above 225 K was fit with the phenomenological Vogel-Fulcher-Tammann relation

$$\tau = \tau_0 \exp\left(\frac{DT_0}{T - T_0}\right), \quad (6)$$

where the constant D quantifies the degree of deviation from Arrhenius behavior, and T_0 is the temperature

at which the relaxation time apparently diverges. The crossing temperature T_x of these two fits is taken as the location of the dynamic crossover. We find $T_x \simeq 220$ K, in reasonable agreement with previous results. We note that the monolayer and full hydration relaxation times cross in the proximity of T_x and can speculate that this may have implications for a dynamic coupling between surface and non-surface water.

Remarkably, the characteristic length scale ℓ (Fig. 6) appears to be relatively insensitive to temperature *and* hydration level, with an average value $\ell_{\text{mono}} = 0.099$ nm and $\ell_{\text{full}} = 0.096$ nm. In Fig. 6, we have also plotted the value of ℓ_{bulk} obtained from QENS measurements of bulk water ($\beta = 1$) [32]. The value of ℓ_{bulk} is less than half that observed in confinement. We postulate that confinement induces a larger value of ℓ . Admittedly, given the non-exponential nature of relaxation in confinement, a direct comparison of ℓ in bulk and confinement may be misleading.

IV. DISCUSSION

The super-Arrhenius behavior observed at high temperatures and full hydration is likely related to enhanced hydrogen bonding and the formation of an open tetrahedral structure, *i.e.*, collective behavior. The strong hydrophilic interactions between water and the silica substrate are believed to prevent surface water from forming an ideal hydrogen bond network. Following previous works, we take the view that the monolayer dynamics are Arrhenius because they depend more strongly on the water-substrate interaction than on the water-water interaction. Our findings are not expected to be unique to the MCM-41 system, although significant differences are expected for strongly hydrophobic substrates.

Yoshida *et al.* [23] have recently measured the coherent dynamics of D_2O confined in MCM-41 using neutron spin-echo (NSE) spectroscopy. In general, their results are consistent with those presented here. However, in the monolayer case, the decay rates measured via NSE are an order of magnitude faster than those measured here. Decay rates measured by these authors at $Q = 14.1$ nm $^{-1}$ are plotted in Fig. 2 for monolayer and full hydration. The origin of this discrepancy between NSE and QENS results is unclear. We note that Takahara *et al.* [33] previously measured QENS spectra of water in MCM-41 at monolayer hydration in larger diameter pores, *i. e.*, not strongly confined, and found that monolayer water relaxes more slowly than full hydration water.

Interestingly, the relaxation times measured by dielectric relaxation (DR) spectroscopy exhibit neither a dynamic crossover nor hydration dependence for water in MCM-41 [11] or in a disordered matrix of silica nanoparticles [34]. The relaxation times measured by QENS and DR can both be related to the shear viscosity in bulk. However, in confinement, the apparent “decoupling” between QENS and DR measurements may imply that this

is no longer the case. Roughly speaking, QENS tends to probe translational motions, whereas DR tends to probe rotational motions. Confinement may induce a decoupling of rotational and translational degrees of freedom.

Mamontov and collaborators [35] have suggested that the dynamic crossover could be a localized phenomenon that only occurs on the length scales probed by QENS. This explanation can also account for the discrepancy between the QENS and DR measurements, since DR corresponds to the limit $Q \rightarrow 0$. Pulsed-gradient spin-echo (PGSE) NMR was previously used to measure the low temperature self-diffusion coefficient of water confined in MCM-41 [10]. This technique essentially probes the hydrogen SISF on much larger length and time scales ($Q \sim \mathcal{O}(10^{-4}) \text{ nm}^{-1}$, $t \sim \mathcal{O}(10) \text{ ms}$) than QENS measurements. Since a dynamic crossover was also observed via PGSE NMR, these measurements may provide a bound on the length scale of this localization.

On the basis of computer simulations, it has recently been argued by Limmer and Chandler [13] that the dynamic crossover observed in fully hydrated pores results from a freezing transition to so-called “crystal-like states”. Below the transition temperature, the observed Arrhenius dynamics are ascribed to the motions of disordered water near the surface of the pore. Both the low temperature monolayer and full hydration dynamics are then associated with activated motions of surface water. That the full hydration times are orders of magnitude larger in this regime can, within this interpretation, be taken as an indication that the non-surface water further impedes the motions of surface water.

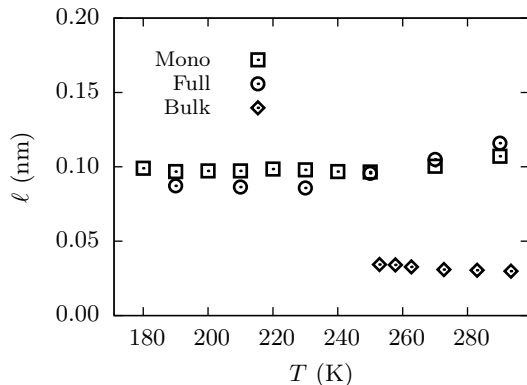


FIG. 6. Characteristic length scale of the diffusion process. The values of ℓ in confinement appear to be fairly independent of temperature and hydration level and significantly larger than the bulk value [32].

Previous work on water confined in MCM-41 [6] and other mesoporous substrates has employed the relaxing cage model (RCM) of supercooled water [36]. In this model, the form of $F_s(t)$ is inspired by ideas from the mode-coupling theory of the glass transition. The decay rate enforced by this model is

$$\Gamma(Q) = \Gamma_0(aQ)^\gamma, \quad (7)$$

where $a = 0.05 \text{ nm}$. This result is in general only applied to the low Q regime. For comparison, we have also fit the decay rates for $Q < 11 \text{ nm}^{-1}$ with Eq. (7). In this restricted Q range, Eq. (7) does indeed provide a satisfactory fit, with qualitative agreement between τ and $1/\Gamma_0$. The dip in γ at low temperatures observed by Faraone *et al.* [6] for the full hydrated case is also found in our fits. This feature is related to the low Q deviations observed for 190 K in Fig. 4.

We have also tried modeling $F_s(t)$ using a sum of two exponentials, as was done in the rutile study of hydration water dynamics [21]. As is typical of the inclusion of an additional fitting parameter, this model often fits the spectra better. However, the two independent decay rates systematically conspire to produce a $F_s(t)$ that reaches a value of $1/e$ on the same timescale as the simpler stretched exponential fits we have used.

V. CONCLUSIONS

We have confirmed that the dynamic crossover observed in the single particle dynamics of fully hydrated MCM-41 is not present at monolayer hydration. The monolayer dynamics appear to be Arrhenius over the full range of experimental temperatures. The monolayer relaxation times are longer than the full hydration times at high temperatures, but become shorter at lower temperatures. This is an indication that the surface-water interactions and the distribution of water on the pore surface change the relaxation phenomena. It is an outstanding question how the dynamics of surface water in fully hydrated pores compare to the dynamics of monolayer hydration water. Computer simulations are likely a promising means of addressing this and related questions.

ACKNOWLEDGMENTS

Research at MIT was supported by the Office of Basic Energy Sciences, U. S. Department of Energy under contract No. DE-FG02-90ER45429. Oak Ridge National Lab, Spallation Neutron Source is supported by the Scientific User Facilities Division, Office of Basic Energy Sciences, U. S. Department of Energy.

-
- [1] C. E. Bertrand, Y. Zhang, and S.-H. Chen, Phys. Chem. Chem. Phys. **15**, 721 (2013).
- [2] G. H. Findenegg, S. Jähnert, D. Akcakayiran and A. Schreiber, Chem. Phys. Chem. **9**, 2651 (2008).
- [3] C. Alba-Simionesco, B. Coasne, G. Dosseh, G. Dudziak, K. E. Gubbins, R. Radhakrishnan and M. Sliwinski-Bartkowiak, J. Phys.: Condens. Matter **18**, R15 (2006).
- [4] B. Webber and J. Dore, J. Phys.: Condens. Matter **16**, S5449 (2004).
- [5] We use the term *deeply-cooled*, as opposed to *supercooled*, to emphasize the fact that strongly-confined water is not in a metastable state.
- [6] A. Faraone, L. Liu, C.-Y. Mou, C.-W. Yen, and S.-H. Chen, J. Chem. Phys. **121**, 10843 (2004).
- [7] J. Swenson, Phys. Rev. Lett. **97**, 189801 (2006).
- [8] S. Cervený, J. Colmenero and A. Alegría, Phys. Rev. Lett. **97**, 189802 (2006).
- [9] S.-H. Chen, L. Liu and A. Faraone, Phys. Rev. Lett. **97**, 189803 (2006).
- [10] F. Mallamace, M. Broccio, C. Corsaro, A. Faraone, U. Wanderlingh, L. Liu, C.-Y. Mou, S.-H. Chen, J. Chem. Phys. **124**, 161102 (2006).
- [11] J. Sjöström, J. Swenson, R. Bergman and S. Kittaka, J. Chem. Phys. **128**, 154503 (2008).
- [12] L. Liu, S.-H. Chen, A. Faraone, C.-W. Yen, and C.-Y. Mou, Phys. Rev. Lett. **95**, 117802 (2005).
- [13] D. T. Limmer and D. Chandler, J. Chem. Phys. **137**, 044509 (2012).
- [14] J. Swenson, R. Bergman and W. S. Howells, J. Chem. Phys. **113**, 2873 (2000).
- [15] J. Swenson, R. Bergman and S. Longeville, J. Chem. Phys. **115**, 11299 (2001).
- [16] O. Sobolev, F. F. Buivin, E. Kemner, M. Russina, B. Beuneu, G. J. Cuello and L. Charlet, Chem. Phys. **374**, 55 (2010).
- [17] F. G. Sánchez, F. Jurányi, T. Gimmi, L. Van Loon, T. Unruh and L. W. Diamond, J. Chem. Phys. **129**, 174706 (2008).
- [18] Y. Kuroda, S. Kittaka, S. Takahara, T. Yamaguchi and M.-C. Bellissent-Funel, J. Phys. Chem. B **103**, 11064 (1999).
- [19] S. Takahara, S. Kittaka, T. Mori, Y. Kuroda, T. Yamaguchi and K. Shibata, J. Phys. Chem. B **106**, 5689 (2002).
- [20] E. Mamontov, J. Chem. Phys. **121**, 9087 (2004).
- [21] E. Mamontov, L. Vlcek, D. J. Wesolowski, P. T. Cummings, J. Rosenqvist, W. Wang, D. R. Cole, L. M. Anovitz, and G. Gasparovic, Phys. Rev. E **79**, 051504 (2009).
- [22] K. Yoshida, T. Yamaguchi, S. Kittaka, M.-C. Bellissent-Funel and P. Fouquet, J. Chem. Phys. **129**, 054702 (2008).
- [23] K. Yoshida, T. Yamaguchi, S. Kittaka, M.-C. Bellissent-Funel, and P. Fouquet, J. Phys.: Condens. Matter **24**, 064101 (2012).
- [24] Y. Zhang, A. Faraone, W. A. Kamitakahara, K.-H. Liu, C.-Y. Mou, Juscelino B. Leão, S. Chang, and S.-H. Chen, Proc. Natl. Acad. Sci. USA **108**, 12206 (2011).
- [25] E. P. Barrett, L. G. Joyner and P. P. Halenda, J. Am. Chem. Soc. **73**, 373 (1951).
- [26] K.-H. Liu, Y. Zhang, J.-J. Lee, C.-C. Chen, Y.-Q. Yeh, S.-H. Chen and C.-Y. Mou (in preparation).
- [27] P. Gallo, M. Rovere, and S.-H. Chen, J. Phys.: Condens. Matter **22**, 284102 (2010).
- [28] W. A. Kamitakahara, A. Faraone, K.-H. Liu and C.-Y. Mou, J. Phys.: Condens. Matter **24**, 064106 (2012).
- [29] E. Mamontov and K. W. Herwig, Rev. Sci. Instrum. **82**, 085109 (2011).
- [30] P. Gallo, M. Rovere and S.-H. Chen, J. Phys.: Condens. Matter **24**, 064109 (2012).
- [31] M.-C. Bellissent-Funel, S.-H. Chen, and J.-M. Zanotti, Phys. Rev. E **51**, 4558 (1995).
- [32] J. Qvist, H. Schober, B. Halle, J. Chem. Phys. **134**, 144508 (2011).
- [33] S. Takahara, M. Nakano, S. Kittaka, Y. Kuroda, T. Mori, H. Hamano, and T. Yamaguchi, J. Phys. Chem. B **103**, 5814 (1999).
- [34] S. Cervený, G. A. Schwartz, J. Otegui, J. Colmenero, J. Luxembourg and Stephan Westermann, J. Phys. Chem. C **116**, 24340 (2012).
- [35] E. Mamontov, A. Faraone, E. W. Hagaman, K. S. Han and E. Fratini, J. Phys. Chem. B **114**, 16737 (2010).
- [36] S.-H. Chen, C. Liao, F. Sciortino, P. Gallo, and P. Tartaglia, Phys. Rev. E **59**, 6708 (1999).